Development of Stimuli-Responsive Mesoporous Silica Nanoparticles for Targeted Cancer Drug Delivery: Synthesis, Characterization, and Ion Incorporation

Klepetsanis Pavlos [1*]

Abstract

Background: The rising incidence of breast cancer has heightened the need for advanced drug delivery systems. Mesoporous silica nanoparticles (MSNs) have emerged as a promising carrier for targeted cancer therapy due to their biocompatibility and ability to provide controlled drug release. Their functionalization, size, and shape allow for enhanced internalization and accumulation in tumors, reducing adverse effects and improving efficacy. Methods: MSNs were synthesized using the sol-gel process with tetraethyl orthosilicate (TEOS) as a precursor. The effects of variables such as pH, stirring rates, and the use of catalysts were studied to optimize particle size and morphology. Zinc and cerium ions were incorporated into the MSN network via post-grafting to enhance therapeutic efficacy. Particles were characterized using FT-IR, XRD, and TEM to analyze size, crystallinity, and composition. Additionally, degradation studies were performed in a physiological medium. Results: Monodispersed MSNs of less than 200 nm were successfully synthesized, with optimal properties achieved at a stirring rate of 600 rpm and pH between 10.5 and 11.5. Zinc and cerium incorporation resulted in enhanced ROS generation, potentially increasing the cytotoxicity towards cancer cells.

Zinc showed increased release in acidic environments, while cerium exhibited pro-oxidant activity in cancer microenvironments. Characterization confirmed successful ion incorporation, with particle sizes maintained below 200 nm. Conclusion: The optimized MSNs with zinc and cerium incorporation demonstrated potential for targeted cancer therapy by inducing oxidative stress in cancer cells while offering controlled drug release. This study highlights the potential of MSNs as a versatile drug delivery platform for oncology.

Keywords: Mesoporous Silica Nanoparticles (MSNs), Stimuli-responsive drug delivery, Cancer therapy, Zinc and cerium ions, Sol-gel synthesis.

Significance | This research advances cancer drug delivery using mesoporous silica nanoparticles, offering precise, stimuli-responsive, and biocompatible therapeutic solutions.

*Correspondence. Klepetsanis Pavlos , University of Patras, Greece
E-mail: klep@upatras.gr

Editor Muhit Rana, Ph.D., And accepted by the Editorial Board Dec 15, 2022 (received for review Oct 04, 2022)

1. Introduction

The incidence rate of breast cancer is estimated to increase by 2% in the UK between 2014 and 2035 (Smittenaar, Petersen, Stewart, & Moitt, 2016). While chemotherapy remains the main treatment modality for cancer, there is a growing demand for stimuli-responsive drug delivery systems that minimize drug adverse effects while providing specific delivery (Du, Lane, & Nie, 2015). Nano-systems with sensitivity towards the cancer microenvironment can facilitate sustained and controlled release of drugs. In addition,

Author Affiliation.
[1] University of Patras, Greece

Please cite this article:
Klepetsanis Pavlos (2022). Development of Stimuli-Responsive Mesoporous Silica Nanoparticles for Targeted Cancer Drug Delivery: Synthesis, Characterization, and Ion Incorporation, Biosensors and Nanotheranostics, 1(1), 1-9, 9852

tumor disorganized vasculature exhibit fenestrations that enable nanoparticles to leave the circulation and accumulate in the tumor because of their small size (Mura, Nicolas, & Couvreur, 2013). Stimuli-responsive nanoparticles (NPs) have great potential to improve therapeutic index by minimizing toxicity while delivering drugs in a passive or active targeting manner (Du et al., 2015; Mura et al., 2013). Furthermore, the global market for nanoparticles in life science is projected to develop up to $79.8 billion by 2019, specifically for drug delivery systems, with oncology being a major focus for nano-pharmaceutical research and development (Highsmith, 2014).

1.1 Mesoporous Silica Nanoparticles (MSNs)

MSNs have emerged as a promising carrier for localized delivery of inorganic and organic drugs. Their mesoporous structure provides a high specific area to volume ratio while enabling sustained and controlled release of drugs (Kwon et al., 2013). They have shown great chemical stability and improved biocompatibility in comparison to other metal oxides and drug carriers such as liposomes and dendrimers (Trewyn, Slowing, Giri, Chen, & Lin, 2007). The stability is attributed to the strong Si–O bond, which makes them independent from covalent linkers for stabilization (Kwon et al., 2013). Furthermore, the abundant presence of silanol groups on the surface with affinity towards phospholipids enables their functionalization and internalization by cells via endocytic pathways (Liong et al., 2008).

1.1.1 Size and Internalisation Mechanism

The morphology and size of particles affect their internalization mechanism. Spherical MSNs can circulate in the body for longer periods and are therefore applicable for targeted delivery compared to rod-shaped particles (Huang, Teng, Chen, Tang, & He, 2010). Furthermore, spherical NPs are reported to internalize in cervical cancer cells and human lung epithelial cells more efficiently (Park & Oh, 2014) due to the high affinity of the ordered silica network towards clathrin-coated endocytic vesicles (Lu, Wu, Hung, & Mou, 2009). Zhu et al. (2013) reported that silica NPs of larger size (308 nm) are taken up via clathrin-mediated endocytosis, while smaller sizes (167.8 nm) were internalized via clathrin and caveolin-mediated pathways in interaction with HeLa cells. Particles smaller than 160 nm showed the most efficient uptake and are applicable for drug delivery (Zhu et al., 2013).

1.1.2 MSNs Sol-gel Synthesis

The sol–gel method is used to produce the silica network through hydrolysis and poly-condensation reactions. A silica precursor such as tetraethyl orthosilicate (TEOS) is hydrolyzed in acidic or basic systems, leading to the formation of Si-O-Si bonds by poly-condensation (Hench & West, 1990; Innocenzi, 2016). The solution of dispersed particles then forms either a gel network by aggregation in an acidic system or monodispersed silica particles in a basic catalyzed system due to repulsion forces between particles generated by hydroxyl ions (Tiwari, Wang, & Wei, 2016). In basic systems, the nucleophilic OH- attacks the silicon atom, creating Si-O-, which then attacks the Si of another Si-O- forming Si-O-Si bonds (Innocenzi, 2016). The use of a catalyst is essential since alkoxysilanes have lower electronegativity and higher Lewis acidity compared to metal alkoxides, making them less reactive towards H2O (Tiwari et al., 2016). Stöber et al. (1968) produced monodispersed silica particles through the sol-gel process using NH3 as the base catalyst. The hydrolysis and condensation reactions are briefly expressed in Eq. 1 and 2 respectively (Zeng, Zhang, Wang, Sang, & Yang, 2015).

The Stöber process can be modified to develop spherical MSNs. The addition of a cationic surfactant such as cetrimonium bromide (CTAB) to the synthesis, followed by its removal via heat treatment, creates pores within particles (Yi et al., 2015; Loryuenyong, Muanghom, Apinyanukul, & Rutthongjan, 2011). CTAB micelles are comprised of hydrophilic heads and hydrophobic tails that self-assemble when dispersed in a liquid colloid. Hydrolysis of TEOS generates hydrophilic silica monomers, which are then attracted by micelles. Consequently, aggregation of neighboring micelles provides the nuclei for the formation of particles while silica is developing a strong framework by hydrolysis and poly-condensation (Yi et al., 2015; Du & He, 2011).

1.1.3 MSNs Synthesis Variables

The systemic variation of reaction variables affects the size, morphology, porosity, and dispersion of particles. Although there are studies to determine how these variables, such as reagent concentration, affect particle properties, reports commonly use different concentrations and processing methods. In addition, variables such as aging and stirring rate have not been studied comprehensively. In order to fulfill the aim of the project, some variables, in particular NaOH and EtOAc concentrations, stirring rate, and aging, were investigated.

1.1.3.1 pH and Basic Catalyst

Figure 1 represents the effect of pH on the condensation rate and charge of silica species, and the effects of pH on silica hydrolysis and condensation rates are shown in Figure 2. pH affects the rates of hydrolysis of silane and their condensation into siloxane bonds. When pH is below the silica isoelectric point, charge density is reduced, and species are positively charged. The increase in pH triggers nucleophilic substitution, increasing the condensation rate. However, above 7.5, silicates' stability and condensation rate decrease (Wu, Mou, & Lin, 2013).

The stable configuration is formed by the interaction of silicates and surfactants, which is stable at higher pH. This stability is attained from 10.5 to 11.5 pH (Wu et al., 2013; Lin & Mou, 2003). The increase in pH is parallel to the increase in catalyst concentration, which produces larger particles by providing nucleation sites as hydrolysis is catalyzed (Ertl, Knözinger, & Weitkamp, 1999).

However, high pH (13) was reported to induce competition between condensation and erosion of the silica network (Chiang et al., 2011).

1.1.3.2 Stirring Rate and Reaction Time

The effect of stirring on particle properties has barely been investigated systematically. While it was reported that stirring rates of 300-700 rpm do not affect particle size (Nozawa et al., 2005), Xun Lv et al. (2016) reported a decrease in sizes from 110 to 38 nm when the rate was increased from 100 to 700 rpm. In addition, stirring rates above 700 rpm did not affect size, suggesting it can mix synthesis adequately (Lv, Zhang, Xing, & Lin, 2016). It is hypothesized that the high local concentration of silica monomers and consequently silica-micelles configurations promote particle growth, resulting in larger MSNs. Conversely, at higher rates, faster diffusion of monomers limits the availability of silica local concentration, and therefore smaller particles are formed (Lv et al., 2016). The 450-650 rpm range leads to the formation of highly organized cubic structures, while at 850 rpm, the peak shapes of XRD are decreased and broadened, indicating poor quality of mesostructure (Kim, Chung, & Lin, 2010). The report on the effect of aging has been inconsistent. Although it is assumed that longer aging promotes particle nucleation growth as condensation proceeds (Kim & Kim, 2003), Chiang et al. (2011) reported an increase in size for up to 4 hours and then a decrease for longer aging (6 and 10 hours), possibly due to erosion of the silica framework.

1.1.3.3 TEOS / CTAB and EtOAc

In the original work by Stöber, the size of particles was not affected by TEOS concentration (Stöber, Fink, & Bohn, 1968). However, Bogush, Tracy, and Zukoski (1988) reported a proportional increase in size with TEOS concentrations. Specifically for MSNs, constant TEOS concentration and an increase in CTAB resulted in a decrease in size by forming more silica nuclei (Xu et al., 2012). Other works suggested an increase in size with TEOS, while highlighting the importance of the TEOS ratio, as an increase in H2O promotes hydrolysis and produces smaller sizes (Rao et al., 2005; Suteewong et al., 2010). The effects of EtOAc concentration and solvent selection were previously investigated (Zeng et al., 2015). It was observed that the addition of EtOAc affected the aggregation rate of particles and their porosity. The use of organic solvents affects the solubility and reaction kinetics, which in turn influences particle morphology.

1.2 Incorporation of Ions as Inorganic Drugs

1.2.1 Zinc

The doping of elements affects the silica network degradability. Bioactive glass is an example of engineered composition with PO4−^-−, Na+^++, and Ca*2*+^*{2+}*2+ affecting the dissolution of the network by forming bonds with non-bridging (NB) oxygens (Jones, 2013). NB oxygen bonds can either relate to Si-O−^-− or Si-OH, with H+^++ acting as network modifiers, decreasing the network connectivity. The size-to-charge ratio and ionic radii of elements define their interaction with the network, either as network formers, modifiers, or intermediates (Chen et al., 2014). Ca*2*+^*{2+}*2+ acts as a modifier, forming NBO bonds; sub-micron silica particles with 15 mol% CaO have shown potential for regenerative medicine. These particles were internalized and degraded in human mesenchymal cells without inducing significant cytotoxicity up to four days (Labbaf et al., 2011).

ZnO nanoparticles (NPs) are reported to induce oxidative stress in cancer cells (Ahamed et al., 2012; Bogdan, Pławińska-Czarnak, & Zarzyńska, 2017). Recent studies on Arginylglycylaspartic acid (RGD)-targeted ZnO NPs demonstrated cytotoxicity toward breast cancer cells. While the response of the cells was heterogeneous, both NPs raised Zn*2*+^*{2+}*2+ concentration in the intracellular environment. Zinc increases reactive oxygen species (ROS) in the acidic microenvironment of tumors, leading to apoptosis (Othman et al., 2016). Muhammad et al. (2011) reported multifunctional ZnO quantum dots (QDs) as a pH-stimuli delivery system, which exhibits a synergistic antitumor effect on cancer cells while delivering doxorubicin. Although ZnO is reported to act as a network modifier in silicate glasses (Xiang et al., 2013), the charge-to-size ratio of zinc is between the limits of modifiers and intermediate oxides. Therefore, zinc plays a bifunctional role in modifying the silica network or forming Si–O–Zn bonds, which is reported to introduce ZnO crystal phases (Liang et al., 2014). The release of silica indicates how zinc interacts with the network since ZnO, as a network former, introduces cross-linking and reduces silica degradability. Zn release was also reported to be 90% higher in acidic environments compared to physiological pH (Chen et al., 2014). A post-grafting method reported to diffuse zinc into the silica network (MCM-41) by 540°C calcination suggested that differences in ionic radii of zinc (0.7 Å) and silicon ions (0.4 Å) induced deterioration of the porous structure (Silvestre-Albero et al., 2008).

1.2.2 Cerium

Cerium, a rare-earth element, has a mixed valence state of Ce*3*+^*{3+}*3+ and Ce*4*+^*{4+}*4+ and can regenerate between both oxidation states. The abundance of point surface defects in CeO*2_22* is associated with oxygen vacancies on the surface of its lattice structure, which enables its recycling (Korsvik et al., 2007). Cerium has shown pro-oxidant properties by generating oxidative stress, leading to the cytotoxicity of cancer cells (Munusamy et al., 2014). The antioxidant characteristics can scavenge superoxide radicals and catalyze the dismutation of the superoxide radical into O*2_22* or H*2_22* O*2_22* (Xu et al., 2013).

CeO*2_22* NPs have shown an inhibitory role on the formation of myofibroblasts, a critical phase in tumor development. Furthermore, their non-cytotoxicity on stromal cells and protection

from oxidative stress underline their application in oncology (Von Montfort et al., 2015). The microenvironment pH affects cerium's role as either a pro- or antioxidant. The acidic environment favors the superoxide radical scavenging activity over the catalase-mimetic H*2_22* O*2_22* scavenging activity, inducing oxidative stress in the microenvironment. The disproportional elevation of reactive oxygen species (ROS) increases mitochondrial oxidative stress, initiating cytochrome C release and activating caspases leading to apoptosis (Xu et al., 2013). The study on post-grafting method used 60 nm silica NPs obtained by a modified Stöber process. Ce(NO*3_33*)*3_33* was dissolved in H*2_22* O and added to a mix of aqueous urea and silica NPs solution, stirred for 3 hours at 85°C, followed by H*2_22* O washing and drying at room temperature. The amount incorporated was 5 wt% for Ce to Si (Munusamy et al., 2014). In addition, CeO*2_22* particles were reported to resist the adverse conditions of cell media by exhibiting superoxide dismutase (SOD) mimetic activity in different pHs (3, 7, and 9) (Korsvik et al., 2007)

2. Materials and Methods

2.1 MSNs Synthesis

The method followed was a modification of Chang et al., using the volume ratio of 500:1:3:5:5 for H_2O: CTAB: NaOH: TEOS: EtOAc. The temperature and stirring rate were set to 70°C and 600 rpm, respectively. 1 g of CTAB (≥98%, Sigma-Aldrich) was added to 500 mL of distilled water in a 1000 mL flask. 3 mL of NaOH (2 mol/L, Merck KGaA) was then added after 5 minutes, followed by drop-wise addition of 5 mL TEOS (99%, ABCR GmbH) after another 5 minutes. Finally, 5 mL of EtOAc (99.5%, Acros Organics) was added after 1 minute, and stirring was stopped after 30 seconds. The solution was then aged for 4 hours, followed by a 40-minute centrifuge to attain a solid pellet of particles. The pellet was then washed with ethanol (99.9%, VWR Chemicals) three times and dried overnight at 60°C. The dried pellet was finally heated to 550°C for 6 hours at a heating rate of 3°C/min. Figure 3 represents the order for the addition of reagents and their interaction.

The particles for the study of stirring rates (400, 600, 800, and 1000 rpm), NaOH, and EtOAc were obtained using the same procedure. The method was progressively optimized to obtain monodispersed MSNs of less than 200 nm. The stirring rate of 600 rpm with the original reported volume ratio provided optimal results. Additionally, stirring for an extra hour after the addition of EtOAc followed by 3 hours of aging resulted in less aggregation.

2.2 Cerium and Zinc Incorporations

A post-grafting method was used to incorporate ions into the MSNs. MSNs were used assuming that after heat treatment, particles are entirely comprised of silica, as FT-IR bending and vibrations confirmed the elimination of CTAB and the presence of Si-O and Si-O-Si bonds. Cerium and zinc salts were measured for $SiO_2(NO_3)_2$ in 1:1 ratio, $SiO_2(NO_3)_3$ in 1:1 and 1:2 ratios, and ultimately 1:1:1 and 1:2:2 ratios for $SiO_2(NO_3)_2(NO_3)_3$ using the number of moles in MSNs for a given amount assuming MSNs consist of SiO_2. 1.6 mg of MSNs were initially mixed with 2 mL of H_2O and sonicated. Additionally, 0.79 g of $Zn(NO_3)_2$ (>98%, Scientific Laboratory Supply) and 1.15 g of $Ce(NO_3)_3$ (99.9%, Sigma Aldrich) were sonicated together and individually with 2 mL of H_2O and added with an additional 1 mL of H_2O to MSNs. The mixture of MSNs and salts was then sonicated, followed by a 15-minute centrifuge and overnight drying at 60°C. Finally, incorporations were heated to 680°C for 3 hours at a heating rate of 3°C/min to eliminate nitrate groups and facilitate the diffusion of ions into the silica network. Figure 4 represents the procedure for the incorporation of ions.

The washing after incorporation was optimized throughout the project. It was either implemented with ethanol three times or HNO_3 followed by H_2O and EtOH, depending on whether Ce or Zn was incorporated. For $SiO_2(NO_3)_3$ and $SiO_2(NO_3)_2(NO_3)_3$ ratios, washing and centrifuge times were as follows: HNO_3 (5 minutes), H_2O (20 minutes), EtOH (20 minutes) followed by overnight drying. The optimal washing procedure for $SiO_2(NO_3)_2$ was achieved with ethanol since nitric acid resulted in the removal of all incorporated ions.

2.3 Physicochemical Characterizations of MSNs

To study the presence of functional groups and confirm the elimination of CTAB and NO_3^-, Fourier transform infrared (FT-IR) spectra were collected on a Bruker Vector 22 FT-IR Spectrometer, in the range of 400-4000 cm^{-1}. X-ray Diffraction (XRD) spectra were also obtained using Cu Kα radiation at 40 kV/40 mA on a Bruker XRD Analyser D2 PHASER powder diffractometer. MSNs and zinc-incorporated particles' data were collected between 10 and 100° 2θ with a dwell time of 1.5 s to study crystallinity. The Ce incorporation was obtained from 10 to 80° 2θ. Additionally, the Scherrer equation was applied to approximate crystallite size for intense peaks using the formula, where τ is the crystallite size, K is the shape factor (~0.9), λ is the X-ray wavelength, β is the line broadening at half the maximum intensity, and θ is the Bragg angle (in degrees). High Score Plus and Data Viewer software enabled measurement of FWHM and peak positions.

The N_2 adsorption/desorption isotherms were obtained using Quantachrome-Autosorb-iQ/MPXR. Specific surface area was measured by applying the multi-point BET method, and pore volume and distribution measurements were obtained using discrete Fourier transform (DFT) and Barrett-Joyner-Halenda (BJH) methods, respectively. The classification of isotherms was according to IUPAC nomenclature. The size was measured by dynamic light scattering (DLS) and zeta potential using ZetaSizer

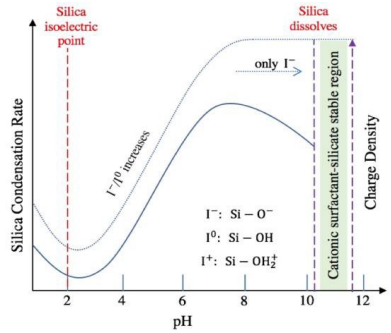

Figure 1. The effect of pH on the condensation rate and silica species charge.

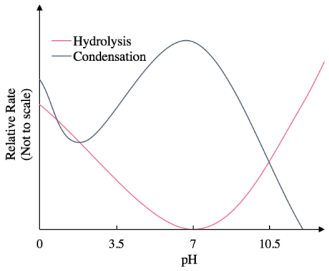

Figure 2. The effects of pH on silica hydrolysis and condensation rate

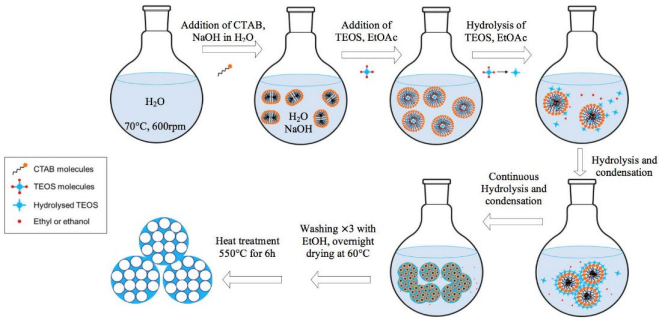

Figure3 . Experimental procedure in MSNs synthesis using CTAB, TEOS, EtOAc, NaOH and H 2 O as reagents

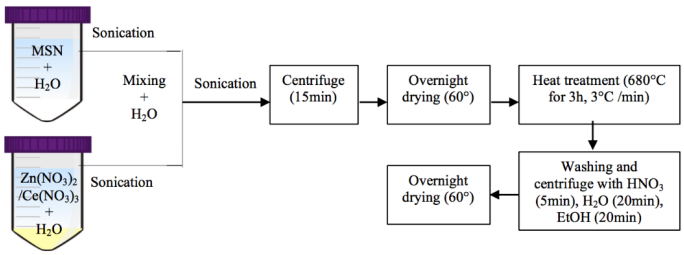

Figure 4. Experimental procedure for incorporation of cerium and zinc into the MSNs.

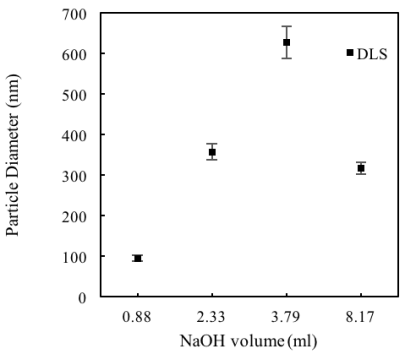

Figure 5. Relationship between NaOH volume and average DLS size of MSNs.

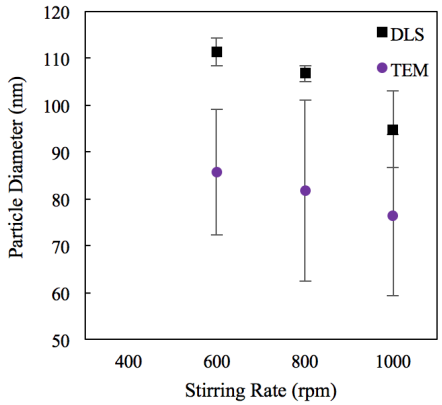

Figure 6. Relationship b etween stirring rate and particle DLS and TEM sizes.

Nano ZS (Malvern). DLS provides the hydrodynamic radius of the particles, which is higher than the TEM radius as the projected area diameter. The size was also measured in bright-field transmission electron microscopy (TEM). Samples were diluted with ethanol and then sonicated for 1 hour. They were then collected on mesh copper grids coated with carbon film. A JEM-2100Plus TEM was used with an operating voltage of 200 kV. Various areas of grids were analyzed, and 50 particles from each sample were measured to calculate the mean diameter. In the case of non-spherical particles, longer and shorter widths were measured in ImageJ software, and the average of 50 particles was calculated. The CeO_2 crystallite sizes were measured using the same procedure. The composition of the incorporations was determined using inductively coupled plasma optical emission spectroscopy (ICP-OES, Thermo Scientific iCAP 6000 series) and EDS detector (Oxford Instrument system) on a JEM-2100Plus TEM was utilized for elemental mapping.

To study particle degradation, Modified Eagle medium (A10490 - MEM alpha, ThermoFisher Scientific) with a pH of 7.4 was used to mimic physiological pH. MEM is used for different cell lines like HeLa B. In addition, human tumors can be cultured in MEM. A protocol was made according to a previous study for silica NPs. 25 mg of particles were suspended in 3 mL of MEM and then poured into SnakeSkin Dialysis Tubing (Thermo Fisher Scientific, 3.5 K MWCO) and placed in a jar filled with MEM to a final volume of 17 mL. Samples were incubated at 37°C in a shaker at 120 rpm. 1 mL was taken from the solution in the jar at 1, 2, 4, 8, 24, 48, 72, 96, 168, 240, and 360 hours, and 1 mL of fresh MEM was added to the jar. The samples were then diluted with 9 mL of H_2O for ICP-OES analysis.

3. Results and Discussion

3.1 Synthesis of MSNs

3.1.1 The Effect of NaOH Volume on Particle Size

The effect of NaOH on the size of particles was studied in DLS. Initially, for 146 mL of H_2O, the amount of NaOH used was 0.88 mL according to Chang et al.'s 500:3 H_2O: NaOH volume ratio. The increase of NaOH resulted in an increase initially and then a decrease for the highest amount of NaOH, as represented in Figure 5. The volume of NaOH was increased from 0.88 mL to 2.33, 3.79, and 8.17 mL relative to the constant 1.46 mL volume of EtOAc.

The measurements correlate with previous studies, suggesting an increase in NaOH catalyzes the hydrolysis of TEOS along with the condensation rate of hydrolyzed monomers, resulting in the growth of particles with bigger size. However, an addition of 8.17 mL NaOH did not further increase the size for the constant aging of 2 hours. A pH of 13 is reported to provide a basic environment for the erosion of the silica network. The pH was measured at 13.8 for 8.17 mL NaOH, and upon addition of EtOAc, it dropped to 13.4 and 12.9, suggesting the erosion mechanism because of the high pH. Therefore, an initial volume of NaOH (0.88 mL) was chosen as it provided the applicable size of particles and was used for further optimization.

3.1.2 The Effect of Stirring Rate on Particle Size

A set of experiments was conducted to investigate the effect of stirring rates on particle size. Particles synthesized at 400 rpm were significantly larger than those synthesized at 600 rpm and 800 rpm. The particle sizes were measured to be larger at 400 rpm (approximately 275 nm) and smallest at 600 rpm (approximately 155 nm). The sizes increased again to about 200 nm at 800 rpm and 230 nm at 1000 rpm (Figure 6). The optimal stirring rate was identified as 600 rpm, yielding the smallest and most uniform particle size.

3.2 Incorporation of Cerium and Zinc

3.2.1 Cerium and Zinc Incorporation Ratios

To incorporate ions into MSNs, a post-grafting method was used. The study focused on different ratios of Ce and Zn. The incorporation of Ce and Zn resulted in increased particle size, as observed in the DLS measurements. For example, the incorporation of Ce (1:1 and 1:2) resulted in average sizes of approximately 180 nm and 210 nm, respectively. The addition of Zn along with Ce (1:1:1 and 1:2:2) resulted in slightly larger sizes (around 220 nm for both). These changes are attributed to the size of the ions and their influence on the network structure of the MSNs.

3.2.2 Characterization of Incorporations

FT-IR and XRD analysis confirmed the successful incorporation of Ce and Zn. FT-IR spectra showed characteristic peaks corresponding to Ce-O and Zn-O bonds. XRD patterns indicated changes in peak positions and intensities corresponding to the incorporation of these ions, confirming their presence in the silica network. The ICP-OES and EDS analysis provided quantitative confirmation of the ion concentrations.

3.3 Degradation Study

The degradation study of MSNs was performed in MEM. The results showed that MSNs degrade over time, with a noticeable release of ions into the solution. The degradation rate was higher in the first 24 hours, with a slower rate thereafter. The data obtained from ICP-OES showed a steady release of ions over time, consistent with the expected behavior of silica-based materials in physiological conditions.

4. Conclusion and Future Works

The development of mesoporous silica nanoparticles (MSNs) as stimuli-responsive drug delivery systems represents a significant breakthrough in cancer therapy. By exploiting the unique properties of MSNs, including their high surface area, pore structure, and ability to incorporate functional elements like zinc and cerium, these nanoparticles offer enhanced targeting and drug release capabilities. The synthesis method, optimized via sol-gel

processes and systematic manipulation of reaction variables such as stirring rate, NaOH, and EtOAc concentrations, ensures the formation of well-defined, monodispersed MSNs with desirable characteristics for drug delivery applications. Furthermore, the incorporation of zinc and cerium ions introduces functionalities that promote oxidative stress in cancer cells, enhancing the therapeutic efficacy while minimizing damage to healthy tissues. This research contributes to the expanding field of nano-pharmaceuticals, with implications for more effective, controlled, and less toxic cancer treatments. Future work will focus on in vivo studies to further validate these findings and optimize the clinical application of MSNs.

This study successfully optimized the synthesis of mesoporous silica nanoparticles (MSNs) by adjusting key parameters such as NaOH volume, stirring rate, and the incorporation of cerium and zinc ions. Using a modified method based on Chang et al., monodispersed MSNs with ideal particle sizes and properties were achieved.

NaOH volume significantly impacted particle size. Initially, increasing NaOH promoted particle growth by enhancing the hydrolysis and condensation of TEOS. However, excessive NaOH caused silica network erosion due to the highly basic environment. An optimal NaOH volume of 0.88 mL produced the best particle sizes. Stirring rates also influenced size, with 600 rpm yielding the smallest and most uniform particles. Deviating from this rate led to larger, less consistent particle sizes.

The post-grafting method effectively incorporated cerium and zinc ions, though it increased particle size. The ratio of cerium to zinc affected final sizes, with both ions together resulting in larger particles than cerium alone. Characterization through FT-IR and XRD confirmed the successful integration of these ions, evidenced by specific peaks indicating Ce-O and Zn-O bonds. Quantitative analysis via ICP-OES and EDS validated the ion concentrations in the MSNs.

In degradation studies using Modified Eagle Medium (MEM), MSNs degraded over time, with an initial rapid release of ions. The release was most pronounced within the first 24 hours, slowing thereafter, consistent with expected nanoparticle behavior in physiological conditions.

Further research could enhance understanding of these MSNs. Investigating ion interactions with the silica network through solid-state nuclear magnetic resonance spectroscopy and exploring how calcination temperatures affect cerium's transition to CeO_2 would be valuable. Additionally, studying one-pot incorporation methods, the stability of these particles in cancerous microenvironments, and assessing their toxicity and efficacy in cancer treatment through cell viability assays could provide insights into their therapeutic potential.

Author contributions

K.P. led the conceptualization, design, and supervision of the study, contributing significantly to data analysis and manuscript preparation. All authors reviewed and approved the final manuscript.

Acknowledgment

Author would tahnkful to their department.

Competing financial interests

The authors have no conflict of interest.

References

Ahamed, M., Javed Akhtar, M., Kumar, S., Khan, M. I., Ahmad, A., & Alrokayan, S. A. (2012). Zinc oxide nanoparticles selectively induce apoptosis in human cancer cells through reactive oxygen species. International Journal of Nanomedicine, 7, 845-857. https://doi.org/10.2147/IJN.S29511

Bogdan, J., Pławińska-Czarnak, J., & Zarzyńska, J. (2017). Nanoparticles of titanium and zinc oxides as novel agents in tumor treatment: A review. Nanoscale Research Letters, 12(1), 41. https://doi.org/10.1186/s11671-017-1725-6

Chen, X., Brauer, D. S., & Karpukhina, N. (2014). 'Smart' acid-degradable zinc-releasing silicate glasses. Materials Letters, 126, 278-280. https://doi.org/10.1016/j.matlet.2014.03.052

Du, J., Lane, L., & Nie, S. (2015). Stimuli-responsive nanoparticles for targeting the tumor microenvironment. Journal of Controlled Release, 219, 205-214. https://doi.org/10.1016/j.jconrel.2015.07.018

Du, X., & He, J. (2011). Spherical silica micro/nanomaterials with hierarchical structures: Synthesis and applications. Nanoscale, 3(10), 3984-3996. https://doi.org/10.1039/C1NR10772J

Ertl, G., Knözinger, H., & Weitkamp, J. (1999). Preparation of solid catalysts. (1st ed.). Weinheim: Wiley-VCH.

Highsmith, J. (2014). Nanoparticles in Biotechnology, Drug Development & Drug Delivery (BIO113B). BCC Research.

Huang, X., Teng, X., Chen, D., Tang, F., & He, J. (2010). The effect of the shape of mesoporous silica nanoparticles on cellular uptake and cell function. Biomaterials, 31(3), 438-448. https://doi.org/10.1016/j.biomaterials.2009.10.047

Innocenzi, P. (2016). The sol to gel transition (1st ed., pp. 12-17). The Sol to Gel Transition.

Jones, J. R. (2013). Review of bioactive glass: From Hench to hybrids. Acta Biomaterialia, 9(1), 4457-4486. https://doi.org/10.1016/j.actbio.2012.09.023

Kim, K., & Kim, H. (2003). Comparison of the effect of reaction parameters on particle size in the formation of SiO2 ,and ZrO2 nanoparticles. Materials Letters, 57(21), 3211-3216. https://doi.org/10.1016/S0167-577X(03)00216-5

Kim, T., Chung, P., & Lin, V. (2010). Facile synthesis of monodisperse spherical MCM-48 mesoporous silica nanoparticles with controlled particle size. Chemistry of Materials, 22(17), 5093-5104. https://doi.org/10.1021/cm100489e

Korsvik, C., Patil, S., Seal, S., & Self, W. (2007). Superoxide dismutase mimetic properties exhibited by vacancy engineered ceria nanoparticles. Chemical Communications, (10), 1056-1058. https://doi.org/10.1039/b616496j

Labbaf, S., Tsigkou, O., Müller, K., Stevens, M., Porter, A., & Jones, J. R. (2011). Spherical bioactive glass particles and their interaction with human mesenchymal stem cells in vitro. Biomaterials, 32(4), 1010-1018. https://doi.org/10.1016/j.biomaterials.2010.10.049

Liang, M. K., Limo, M. J., Sola-Rabada, A., Roe, M. J., & Perry, C. C. (2014). New insights into the mechanism of ZnO formation from aqueous solutions of zinc acetate and zinc nitrate. Chemistry of Materials, 26(14), 4119-4129. https://doi.org/10.1021/cm501561h

Lv, X., Zhang, L., Xing, F., & Lin, H. (2016). Controlled synthesis of monodispersed mesoporous silica nanoparticles: Particle size tuning and formation mechanism investigation. Microporous and Mesoporous Materials, 225, 238-244. https://doi.org/10.1016/j.micromeso.2016.02.036

Munusamy, P., Sanghavi, S., Varga, T., & Suntharampillai, T. (2014). Silica supported ceria nanoparticles: A hybrid nanostructure to increase stability and surface reactivity of nano-crystalline ceria. RSC Advances, 4(17), 8421-8430. https://doi.org/10.1039/C3RA46323B

Mura, S., Nicolas, J., & Couvreur, P. (2013). Stimuli-responsive nanocarriers for drug delivery. Nature Materials, 12(11), 991-1003. https://doi.org/10.1038/nmat3776

Nozawa, K., Gailhanou, H., Raison, L., Panizza, P., Ushiki, H., Sellier, E., Delville, J., & Delville, M. (2005). Smart control of monodisperse Stöber silica particles: Effect of reactant addition rate on growth process. Langmuir, 21(4), 1516-1523. https://doi.org/10.1021/la047361a

Othman, B., Greenwood, C., Abuelela, A., Bharath, A., Chen, S., Theodorou, I., Douglas, T., Uchida, M., Ryan, M., Merzaban, J., & Porter, A. (2016). Targeted cancer therapy: Correlative light-electron microscopy shows RGD-targeted ZnO nanoparticles dissolve in the intracellular environment of triple negative breast cancer cells and cause apoptosis with intratumor heterogeneity. Advanced Healthcare Materials, 5(11), 1248-1260. https://doi.org/10.1002/adhm.201500670

Park, J., & Oh, N. (2014). Endocytosis and exocytosis of nanoparticles in mammalian cells. International Journal of Nanomedicine, 9, 51-60. https://doi.org/10.2147/IJN.S39582

Rao, K. S., Srinivasa, R. K., Reddy, K. S., & Khan, M. S. (2005). A novel method for synthesis of silica nanoparticles. Journal of Colloid and Interface Science, 289(1), 125-131. https://doi.org/10.1016/j.jcis.2005.03.067

Silvestre-Albero, J., Sepúlveda-Escribano, A., & Reinoso, F. (2008). Preparation and characterization of zinc containing MCM-41 spheres. Microporous and Mesoporous Materials, 113(1-3), 362-369. https://doi.org/10.1016/j.micromeso.2008.01.006

Smittenaar, C., Petersen, K., Stewart, K., & Moitt, N. (2016). Cancer incidence and mortality projections in the UK until 2035. British Journal of Cancer, 115(9), 1147-1155. https://doi.org/10.1038/bjc.2016.295

Stöber, W., Fink, A., & Bohn, E. (1968). Controlled growth of monodisperse silica spheres in the micron size range. Journal of Colloid and Interface Science, 26(1), 62-69. https://doi.org/10.1016/0021-9797(68)90272-5

Suteewong, T., Sai, H., Lee, J., Bradbury, M., Hyeon, T., Gruner, S., & Wiesner, U. (2010). Ordered mesoporous silica nanoparticles with and without embedded iron oxide nanoparticles: Structure evolution during synthesis. Journal of Materials Chemistry, 20(36), 7807-7816. https://doi.org/10.1039/c0jm01342j

Tiwari, A., Wang, R., & Wei, B. (2016). Advanced surface engineering materials (1st ed., pp. 36-42). Beverly, MA: Scrivener Publishing.